

Marine energy supported multi-energy system planning and operation optimization for sustainable coastal community[☆]

Nana Duah ^a , Yang Chen ^{b,*}, Om Prakash Yadav ^a , Jun Chen ^c

^a Department of Industrial and Systems Engineering, North Carolina A&T State University, Greensboro, NC, USA

^b Computational Sciences and Engineering Division, Oak Ridge National Laboratory, 1 Bethel Valley Rd., Oak Ridge, TN 37831, USA

^c Department of Electrical and Computer Engineering, Oakland University, Rochester, MI, USA

ARTICLE INFO

Keywords:

Coastal community
Marine energy
Multi-energy system
Capacity planning
Operation optimization

ABSTRACT

The growing need for sustainable energy solutions in coastal areas necessitates the development of integrated systems that leverage abundant marine resources. In this study, a standalone Marine Energy Supported Multi-Energy System (MRE-MES) is designed for sustainable coastal community development, utilizing renewable marine resources, including offshore wind, wave, and solar energy, to address the energy needs of electricity, heat, freshwater, and hydrogen. The proposed MRE-MES incorporates a co-optimization model that simultaneously balances capacity planning and operational efficiency to minimize costs and environmental impacts. The system is tested under different renewable energy penetration levels and demand uncertainties, using a two-stage stochastic programming to account for variability in renewable resources and consumption needs. The experimental results indicate that in the optimal system capacity configuration, the percentage of total renewable energy generation is around 80 %, with or without capacity limitation constraints on PV, water tank, and hydrogen storage. Compared to the worst-case scenario in Monte Carlo experiments, two-stage stochastic optimization results in a more robust decision that effectively mitigates the risks posed by future uncertain demand conditions. The findings highlight the viability of marine energy for providing a resilient, comprehensive energy solution to coastal communities.

1. Introduction

Coastal communities in the United States (U.S.) are expanding rapidly, with approximately 40 % of the country's population residing in these areas [1]. Due to their geographical location, these communities face significant economic, social, and environmental challenges, making them vulnerable to the effects of climate change [2,3]. Renewable energy technologies, particularly marine renewable energy (MRE) which includes offshore wind and ocean energy, have emerged as promising solutions, offering resilience, environmental sustainability, and benefits in energy security, affordability, and socioeconomic advancement [4]. MRE is characterized by its reliability, low risk factors, and potential capacity, which may exceed the current world electricity demand, as suggested by many studies. It offers a valuable source of clean electricity,

potable desalinated water, and thermal energy to coastal communities [5,6].

Among the various forms of MRE, offshore wind energy is the only commercially deployed marine renewable energy with wide-scale adoption [7], while tidal and wave energy stand out for their relatively higher technological maturity within ocean energy sources. While still in earlier development stages compared to other renewable energy sources, waves and tides possess immense potential for sustainable energy generation. For instance, the U.S. Energy Information Administration estimates that the annual wave energy potential off the coast is approximately 2.64 trillion kWh, equivalent to 64 % of the total utility-scale electricity generation in the United States in 2021 [8]. Theoretically, wave energy has superior potential compared to other MRE due to its higher

[☆] This manuscript has been authored in part by UT-Battelle LLC under contract DE-AC05-00OR22725 with the US Department of Energy (DOE). The US government retains and the publisher, by accepting the article for publication, acknowledges that the US government retains a nonexclusive, paid-up, irrevocable, worldwide license to publish or reproduce the published form of this manuscript, or allow others to do so, for US government purposes. DOE will provide public access to these results of federally sponsored research in accordance with the DOE Public Access Plan (<http://energy.gov/downloads/doe-public-access-plan>).

* Corresponding author.

Email address: cheny4@ornl.gov (Y. Chen).

density, ranging from 2 to 3 kW/m² [9] compared to hydropower (0.2 kW/m²) [10] and wind energy (0.002–0.005 kW/m²) [11] making it a promising candidate for sustainable energy generation in coastal regions. Harnessing these abundant MRE resources holds great promise for transitioning towards a low-carbon economy, reducing CO₂ emissions from electricity generation, and advancing a sustainable energy future [12,13]. The advancement of MRE will be essential for the U.S. to achieve its goal of 100 % renewable energy and meet associated climate change targets by 2035 [5].

To fully realize this potential, particularly in coastal regions where these resources are most accessible, MRE development must go beyond technical deployment. Integrated systems that consider local needs and contexts, aligning technological innovations with social and environmental priorities, are required. The Meaningful MRE development framework proposed by Caballero et al. [14] emphasizes the importance of energy justice in guiding MRE deployment. This approach ensures that MRE projects not only provide clean energy but also address historical inequities, support local livelihoods and promote community resilience. However, one major limitation of MRE is that it is not cost-effective for long-distance inland energy transmission due to high cost of building and maintenance cost, making it primarily suitable for coastal communities [15].

Beyond electricity, coastal communities have diverse needs, including hydrogen, heat, and freshwater [16]. In transportation sector, the International Maritime Organization's 2020 regulations limit sulfur content in ship fuel from 3.5 % to 0.5 %, and to 0.1 % in Emissions Control Areas near U.S. and European Union coasts. With these stricter standards, hydrogen and its carriers emerge as promising alternatives to bunker fuel. Hydrogen use in marine vessels, ports, and associated equipment could reduce carbon dioxide and other emissions while fostering regional infrastructure development [15]. Approximately one-third of the U.S. population resides in coastal areas, a figure expected to rise with continued urbanization [17]. These communities rely heavily on ocean resources to support various physical and social well-being requirements [18]. For instance, the Delta River is a crucial water source, serving approximately 66 % of California's population and irrigating over 3 million acres of farmland [19]. As population growth continues, the demand for energy especially for heating and hydrogen is projected to increase accordingly. The U.S. hydrogen demand is projected to grow significantly, from approximately 11.5 million metric tons (MMT) in 2021 [20] to 50 MMT by 2050 [21]. This rising demand will have substantial implications for coastal regions, where hydrogen production and infrastructure are likely to expand. To better capitalize on abundant energy resources and integrate various forms of demands such as electricity, heating, freshwater, and hydrogen in a coordinated manner, the previously developed concept “multi-energy system” is adopted here and building marine renewable energy supported multi-energy system (MRE-MES) that operates with minimal reliance on external grids is essential for coastal communities as such a system would meet their comprehensive energy and water needs.

2. Literature review

Currently, the related research can be categorized into two main streams: one category focuses on MRE-supported microgrids, and the other on MES operation without involving marine renewable energy, with very few studies conducted on MRE-MES specifically. The two categories are reviewed in the following paragraphs.

On one hand, numerous studies have explored optimal operation strategies for MRE-supported microgrids to enhance efficiency, minimize costs, and reduce CO₂ emissions. For instance, Aktaş and Kirçicek [22] present a novel energy management strategy for hybrid renewable systems combining offshore wind, marine current, batteries, and ultracapacitors to ensure stable power. The developed algorithm dynamically controls power flow, minimizes fluctuations, and enhances system reliability. Similarly, optimal economic dispatch in an energy hub with tidal

energy is studied in [23], where a mixed-integer linear programming model is utilized to minimize operational and environmental costs. A multi-objective model is presented in [24] to address the environmental and economic optimization of microgrids incorporating tidal energy and energy storage, focusing on the effective use of renewable resources for sustainable power supply. The modified bird mating optimizer algorithm is utilized to manage energy dispatch, reducing both operational costs and emissions. The study highlights the complementarity of tidal and photovoltaic resources, demonstrating that a microgrid utilizing both can reliably meet load demands. Optimal scheduling in a microgrid integrating tidal power generation to enhance renewable energy use while reducing costs is examined in [25]. The study focuses on a microgrid near Darwin, Australia, where tidal power output is forecasted for an operational period of 14 days (a half lunar cycle) based on tidal current data. A particle swarm algorithm is adopted to solve this non-linear scheduling model effectively. Comparative analysis shows that the developed algorithm outperforms traditional optimization methods, such as particle swarm and grey wolf algorithms, in handling power fluctuations and meeting load demands. Reference [26] tackles the challenge of optimizing real-time energy management in wave-powered ocean observation systems, which face constraints due to variable wave resources and the need to avoid oversizing energy storage and generation. A forecast-based stochastic optimization method, utilizing Markov decision processes, is used to manage load demand based on wave forecasts. The study demonstrates that Markov process-driven decisions significantly reduce the required battery and wave energy converter sizes compared to non-forecast-based methods. Ceusters et al. [27] benchmarked Model Predictive Control (MPC) against state-of-the-art reinforcement learning (RL) algorithms in simulated MES environments to minimize operational costs. Their results showed that RL agents not only outperformed realistic MPC under uncertainty but also surpassed perfect foresight MPC in simpler MES configurations. The issue of fluctuating wave power is addressed in [28] for grid-connected wave energy parks by implementing a hybrid energy storage system combining batteries and supercapacitors. A dynamic rate limiter in the control system manages high- and low-frequency power demands, directing rapid fluctuations to supercapacitors to reduce battery stress. Results show that this method enhances energy stability, prolongs battery life, and supports renewable grid integration effectively.

On the other hand, the operation of MES with various combinations of electricity, thermal energy, hydrogen, fresh/potable water, etc., has also been extensively studied. Reference [29] reviews the integration of electricity, gas, and water systems in multi-carrier energy networks, highlighting the economic and environmental benefits of integrated management, particularly through optimized dispatch and scheduling. An energy system integrating hydrogen production and distribution with a combined cooling, heating, and power system powered by substantial wind energy is proposed in [30], achieving an energy efficiency of 72 % and a wind power utilization rate of 92.6 %. In pursuit of carbon neutrality, Wen and Aziz [31] design a multi-energy hub incorporating hydrogen and ammonia as energy carriers for cost-effective renewable integration and large-scale storage. Two pathways, power-to-gas-to-power (P2X2P) and biomass-to-gas-to-power (B2X2P), are proposed, with scheduling controlled through mixed-integer linear programming and a modified double deep Q-network reinforcement learning method, demonstrating B2X2P as more profitable and P2X2P as more operationally flexible. Franzoso et al. [32] conducted a study applying Deep RL to MES optimization under high renewable energy penetration. Their work emphasizes the coordinated control of key technologies, including combined heat and power (CHP), Battery Energy Storage Systems Heat Pumps, and Power-to-Gas. This approach addresses the increasing complexity of MES operations, which are influenced by interconnected two-way energy flows across electricity, heating, and gas networks. An integrated scheduling model for optimal dispatch of cooling, heating, power, gas, and water demand is examined within an energy-water microgrid in [33], where a multi-objective two-stage

stochastic optimization model minimizes total cost and potable water extraction, solved by the epsilon-constraint method.

While these operational studies effectively reduce costs and CO₂ emissions, their impact is limited from a life-cycle perspective due to the fixed capacity sizes of energy components established during the early design stages [34]. Consequently, determining the optimal size of each energy component before construction becomes essential to achieving long-term performance, adaptability, and sustainability. General capacity configuration or sizing strategies commonly employ several key approaches: multi-objective or multi-criteria optimization for balancing conflicting objectives, response surface methodology for iterative model refinement, and simultaneous design and operation optimization (or co-optimization) to account for future operating conditions in the design process. Additional methods, such as surrogate modeling, are also frequently used to enhance efficiency and precision.

Several studies have addressed capacity sizing for MES. For example, a modified combination of the grey wolf optimization algorithm and the sine-cosine algorithm is employed [35] to determine the number of subsystems in a stand-alone hybrid renewable energy system comprising wind, solar panels, bio-waste units, and storage, designed to meet both electrical and thermal demands by minimizing the levelized cost of energy and total annualized net present cost. The optimal configuration of an off-grid hybrid energy system including a wind, fuel cell, alkaline electrolyzer, battery, and supercapacitor bank is investigated [36], employing Non-dominated Sorting Genetic Algorithm to balance cost and supply reliability. Similarly, Jahangir et al. [37] considered the capacity design of PV, wind, and wave energy converters to meet the electricity demand of coastal communities, with a sensitivity analysis conducted to refine subsystem capacities by adjusting design parameters, allowing the determination of the most cost-effective and reliable configurations under both on-grid and off-grid scenarios. A multi-generation system designed for remote communities in [38] incorporates wind, solar, hydrogen storage, and cooling technologies, with capacities based on energy and exergy performance.

Significant progress has been made in the literature on MES. However, none of the existing studies reviewed above simultaneously optimize capital investment and operational costs. These two aspects are inherently interdependent: the optimal operating strategy depends on the system design, and the most cost-effective design can only be realized when operations are jointly considered. Therefore, it is essential to address both dimensions for long-term planning and realistic assessments. Only a limited number of studies have explored this integration, and those that have are generally restricted in scope. For instance, Wang et al. [39] proposed a two-stage robust planning model for offshore microgrids that integrates tidal energy and desalination, optimizing both investment and operations under uncertainty. Study [40] introduced a combined surrogate modeling and dynamic programming framework for the design and operation of a multi-generation MES. In [41], a PV-wind-battery-thermal storage hybrid power system was modeled through a multi-objective planning-operation co-optimization framework, aiming to minimize both the net present cost and the loss of power supply probability. Similarly, Liu et al. [42] present a bi-level co-optimization framework for a PV-wind-hydrogen MES, linking capacity planning at the upper level with operational strategies at the lower level.

Overall, current MES research largely emphasizes either design or operation in isolation, with relatively few studies addressing co-optimization. Although these studies link design and operation, they are usually restricted to a few carriers, such as electricity, desalination, or hydrogen [39,42], or rely on conventional renewables such as PV and onshore wind [40–42]. Consequently, these studies overlook emerging MRE, which holds significant potential for enhancing the sustainability and resilience of coastal energy systems. This paper addresses these gaps by introducing a generalized framework for standalone MRE-MES configurations that simultaneously optimize capacity investment and operational costs. The proposed framework is adaptable to the

distinct energy demands and renewable resource profiles of coastal regions. By integrating MRE with multiple carriers, including electricity, heat, freshwater, and hydrogen, the model provides a holistic solution that goes beyond the cost-centric focus of most existing MES studies to date. In addition to delivering cost efficiency, the framework explicitly enhances resilience and energy security, addressing vulnerabilities in coastal communities. Its generalized design ensures flexibility, allowing emerging technologies to be integrated or system components to be reconfigured, making it applicable across diverse contexts while filling critical gaps in the literature. To harness marine renewable resources in conjunction with diverse local multi-energy demands in coastal areas, this research contributes in the following ways: (1) A comprehensive standalone MRE-MES system is proposed, integrating energy conversion and storage processes for various demands (electricity, heating, hydrogen, and freshwater) in a coordinated manner. (2) A generalized co-optimization model of capacity sizing and operation is established to simultaneously balance capital investment during the design phase with economic and carbon emission performance in subsequent operations. The model is general in the sense that it is not tied to a single case study but can be adapted to diverse coastal areas, each with distinct energy demands and marine renewable resource availability. (3) To address uncertainties in marine renewables and fluctuating demands, Monte Carlo simulations are conducted, and the developed model is extended using two-stage stochastic programming, with the value of the stochastic solution calculated.

The remainder of this paper is structured as follows: Section 3 introduces the configuration of the proposed standalone MRE-MES. Section 4 presents the mathematical model of the system components and the associated parameter values. Section 5 details the developed co-optimization planning model. Section 6 describes the case study and scenario settings used in the analysis. Section 7 presents and discusses the results, and Section 8 concludes the study by highlighting the main findings, limitations, and directions for future research.

3. System description

The proposed system scheme of standalone MRE-MES designed for coastal areas is illustrated in Fig. 1.

The system is divided into four distinct phases, each contributing to a comprehensive energy solution for coastal communities, addressing various demands including residential water, electricity, thermal energy, and hydrogen. In Phase 1, natural resources such as wind, solar, wave energy, natural gas, and seawater are utilized as the primary inputs for the system. In Phase 2, these resources are converted and processed: wind turbines (WT), photovoltaic arrays (PV), and wave energy converters (WEC) generate renewable electricity, while the combined heat and power (CHP) unit uses natural gas to produce both electricity and thermal energy. Additionally, seawater is processed into potable water through a desalination plant, and an electrolyzer utilizes electricity and seawater to produce hydrogen. In Phase 3, energy storage systems act as buffers to optimize the balance between supply and demand. Specifically, purified water is stored in a water tank, electrical energy in batteries, thermal energy in thermal storage units, and hydrogen in a hydrogen tank. Finally, Phase 4 involves distributing the stored energy and resources to meet the diverse needs of coastal communities, including residential electricity, thermal energy, potable water, and hydrogen.

4. Mathematical model of the MRE-MES components

4.1. Renewable energy generation

4.1.1. Wind energy system

Wind power is generated by turbine blades harnessing the kinetic energy of the wind, converting it into mechanical energy, which is then transformed into electricity by an alternator [43]. The total active power generated by the WTs at hour t can be calculated using Eq. (1) [35].

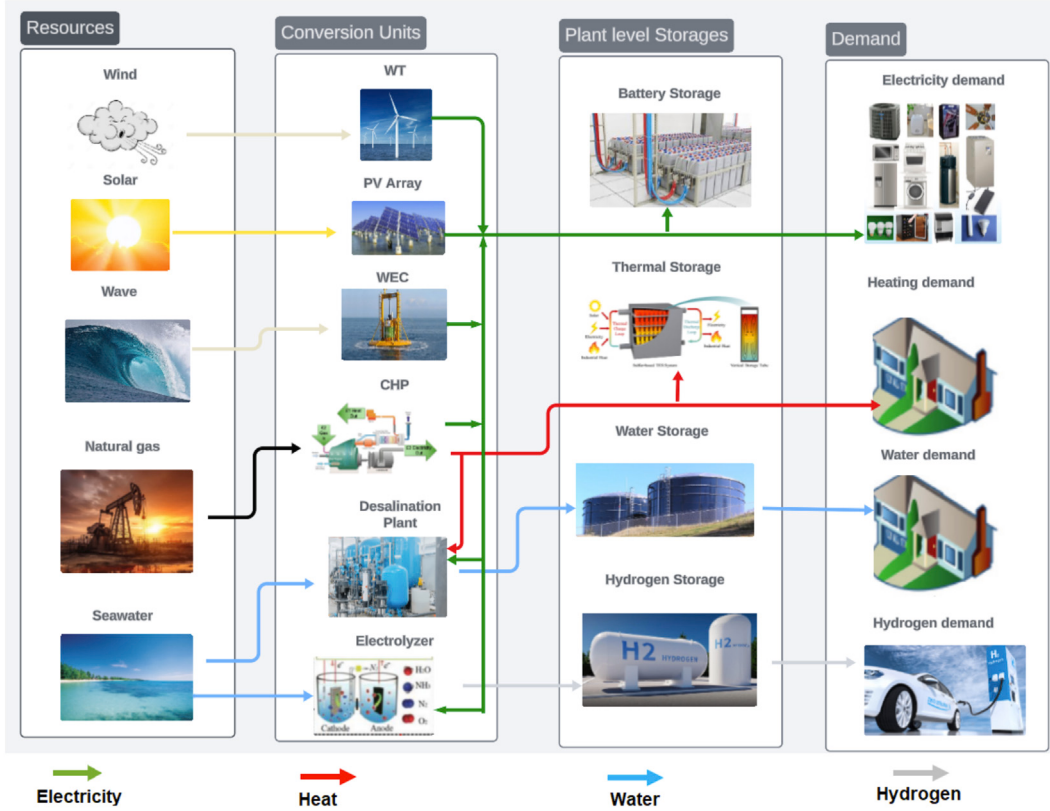


Fig. 1. The system scheme of MRE-MES for coastal community.

Table 1
Wind energy system parameters.

Parameter	Symbol	Value	Unit	Reference
Unit cost	U_W	1,300,000	\$/MW	[44,45]
Rated power	R_W	0.5	MW	[46]
Cut-in speed	I	3	m/s	[46]
Rated speed	Λ	13	m/s	[46]
Cut-off speed	Φ	25	m/s	[46]
Maintenance cost	M_W	$20,000 \cdot N_W \cdot R_W$	\$/year	[47,48]

The wind turbine operates in different regions: if the wind velocity V_t (m/s) is less than the cut-in velocity I or exceeds the cut-off velocity Φ , no power is generated. If wind velocity is greater than the cut-in velocity but lower than the rated velocity Λ , the generated power can be modeled as linearly increasing up to its rated power R_W . The number of WTs, N_W , is a decision variable in the capacity planning stage, and the corresponding capital cost C_W is calculated using Eq. (2), where U_W is the unit cost of a wind turbine. The relevant parameters of WT are listed in Table 1.

$$pW_t = \begin{cases} N_W \cdot R_W & \Lambda \leq V_t \leq \Phi \\ N_W \cdot R_W \cdot \frac{V_t - I}{\Lambda - I} & I \leq V_t \leq \Lambda \\ 0 & V_t \leq I \text{ or } V_t \geq \Phi \end{cases} \quad (1)$$

$$C_W = N_W \cdot U_W \quad (2)$$

4.1.2. Photovoltaic system

PV modules convert sunlight into electrical power, providing a promising solution for electricity generation and reducing carbon emissions. The output power of PV modules primarily depends on the

Table 2
PV system parameters.

Parameter	Symbol	Value	Unit	Reference
Derating factor	τ_p	90	%	[49]
Efficiency	η_p	15	%	[49]
Temp. coefficient	γ_p	0.45	%/°C	[49]
Unit cost	U_p	30	\$/m²	[49]
Maintenance cost	M_p	$13,200 \cdot S_p \cdot 0.0002$	\$/year	[50–52]

intensity of solar radiation striking the module surface and the ambient temperature. The output power of the PV system at hour t can be calculated using Eq. (3) [15], where Ω_t (kWh/m²) refers to the solar irradiance on a tilted surface, τ_p is the derating factor (in %) accounting for the effects such as shading, snow cover, cloud and dust, and η_p represents the efficiency of the PV system. The total PV surface area, S_p , is a decision variable in capacity planning. The temperature coefficient is denoted by γ_p , while T_t is ambient temperature in Celsius. The investment in the PV system, C_p , can then be calculated using Eq. (4), where U_p is the unit cost of the photovoltaic system. The relevant parameters of the PV module are listed in Table 2.

$$pS_t = \Omega_t \cdot \tau_p \cdot \eta_p \cdot S_p \cdot [1 - \gamma_p \cdot (T_t - 25)] \quad (3)$$

$$C_p = S_p \cdot U_p \quad (4)$$

4.1.3. Wave energy converter

The WEC harnesses the energy from ocean waves and converts it into electricity. The wave power output, pV_t , can be estimated using Eq. (5) [53,54] under deep water conditions, where ρ is the seawater density, g is gravitational acceleration, and H_t is the significant wave height. The overall efficiency of the WEC, denoted by η_V , depends on the specific

Table 3
WEC parameters.

Parameter	Symbol	Value	Unit	Reference
Gravitational Acc.	g	9.8	m/s^2	
Seawater density	ρ	1.028	kg/m^3	
Overall Efficiency	η_V	40	%	[58]
Wave period	T_V	2	s	[58,59]
Wavefront length	L_V	120	m	[58,59]
Unit cost (Pelamis 0.75 MW)	U_V	3,000,000	\$/MW	[58,59]
Maintenance cost	M_V	$0.016 \cdot C_V$	\$/year	[59]

technology used [55,56]. The wavefront length is given by L_V , and T_V is the wave period. This formulation captures the key environmental and design factors influencing wave power generation. Because wave energy availability varies by geographic location and time [57], the model enables the dynamic computation of power output based on time-series wave height data. It assumes deep-water conditions, which are commonly used for offshore wave energy deployments [57]. The converter number in the WEC array, N_V , is a decision variable in capacity planning stage, which leads to the calculation of the investment cost, C_V , using Eq. (6), where U_V is the unit cost of WEC. Note that the power output pV_t calculated in Eq. (5) is in Watts and needs to be converted to MW. The relevant parameters of the WEC are listed in Table 3.

$$pV_t = N_V \cdot \eta_V \cdot \frac{\rho \cdot g^2 \cdot T_V \cdot H_t^2 \cdot L_V}{32\pi} \quad (5)$$

$$C_V = N_V \cdot U_V \quad (6)$$

Therefore, the total renewable power output, pR_t , can be summed up by Eq. (7).

$$pR_t = pW_t + pS_t + pV_t \quad (7)$$

4.2. Water desalination

The reverse osmosis desalination plant consumes electricity to propel seawater through a reverse osmosis membrane to produce freshwater [15]. The total power consumption of the desalination plant, pD_t , is determined by the product of the water flow rate, wf_t , and the desalination specific energy consumption, ds_t (kWh/m^3), as shown in Eq. (8). The specific energy consumption, ds_t , is itself a function of wf_t , as given in Eq. (9).

$$pD_t \cdot 1000 = ds_t \cdot wf_t \cdot N_O \quad (8)$$

$$ds_t = 2.05 \cdot 10^{-5} \cdot C_0 \cdot \frac{2 - R}{2 \cdot (1 - R)} + 2.78 \cdot 10^{-7} \cdot R_m \cdot wf_t \quad (9)$$

$$wf_t \leq \overline{WF} \quad (10)$$

$$cd = 4472.94 \cdot (24 \cdot \overline{WF})^{-0.125} \quad (11)$$

$$C_D = cd \cdot 24 \cdot \overline{WF} \cdot N_O \quad (12)$$

Water flow rate, wf_t , in each hour t is limited by an hourly upper bound \overline{WF} . The specific cost, cd ($$/\text{m}^3$), depends on the daily water flow rate capacity, as described in Eq. (11) [60]. Consequently, the capital cost of the desalination plant, C_D , is obtained using Eq. (12), where N_O is the number of reverse osmosis modules, R is the water recovery ratio of the process, R_m is the membrane resistance, and C_0 is the initial salt concentration of the feed water. The relevant parameters of desalination plant are listed in Table 4.

4.3. CHP system

CHP systems can simultaneously generate electricity and thermal energy, whereas gas boilers are heat generators. The electrical and thermal generation are interdependent and cannot be controlled separately [62].

Table 4
Desalination system parameters.

Parameter	Symbol	Value	Unit	Reference
Initial salt concentration	C_0	36,000	ppm	[60]
Water recovery ratio	R	0.55	—	[60]
Membrane resistance	R_m	33.95	Pa-Sec/m	[60]
Max flow rate	\overline{WF}	458.33	m^3/h	[60]
Maintenance cost	M_D	$0.02 \cdot C_D$	\$/year	[61]

Table 5
CHP system parameters.

Parameter	Symbol	Value	Unit	Reference
Gas calorific value	V_G	0.0097	MWh/m^3	[66]
Turbine efficiency	η_T	35	%	[66]
Heat loss coefficient	η_L	50	%	[66]
Heat exchanger Coefficient	η_X	50	%	[66]
Boiler efficiency	η_Q	65	%	[66]
Maintenance cost (turbine)	M_G	$0.03 \cdot C_G$	\$/year	[65]
Maintenance cost (boiler)	M_B	62.63	\$/MW/year	[65]

The energy generated for both heat and power by the CHP can be calculated based on Eqs. (13)–(15) [63], where pT_t and qT_t are power and thermal energy generated together by gas turbine, and qB_t is the thermal energy generated by gas boiler. gT_t and gB_t denote the gas inputs for the gas turbine and boiler respectively. V_G is the lower calorific value of gas. η_T represents the generation efficiency of gas turbine, while η_Q is the thermal generation efficiency of the gas boiler. Additionally, η_L is the heat loss coefficient of gas turbine, and η_X is the heat exchanger coefficient.

$$pT_t = gT_t \cdot V_G \cdot \eta_T \quad (13)$$

$$qT_t = \eta_X \cdot pT_t \cdot \frac{1 - \eta_T - \eta_L}{\eta_T} \quad (14)$$

$$qB_t \leq gB_t \cdot V_G \cdot \eta_Q \quad (15)$$

$$pT_t \leq R_G \quad (16)$$

$$qB_t \leq R_B \quad (17)$$

$$C_G = 13,885.57 \cdot R_G^{0.57} \quad (18)$$

$$C_B = 29,000 \cdot R_B \quad (19)$$

The power capacity R_G and thermal capacity R_B of the gas turbine and gas boiler respectively, are decision variables in the system capacity planning stage. Correspondingly, the capital costs of the gas turbine C_G and gas boiler C_B (in $$/\text{MW}$), can be calculated based on the formula in Eqs. (18) and (19) [64,65]. The relevant parameters of CHP are listed in Table 5.

4.4. Electrolyzer

The electrolyzer consumes electricity to generate hydrogen from seawater. Hydrogen production can be determined using Eq. (20) [67], where hf_t represents the hydrogen production flow, η_Z is the efficiency of the electrolyzer, pZ_t is the power input for a single electrolyzer unit, and PH is the power-to-hydrogen conversion factor. The number of electrolyzer units, N_Z , is a decision variable when planning the capacity of the plant.

$$hf_t = \eta_Z \cdot pZ_t \cdot PH \cdot N_Z \quad (20)$$

$$\underline{\alpha} \cdot R_Z \leq pZ_t \leq R_Z \quad (21)$$

$$C_Z = N_Z \cdot R_Z \cdot ce \quad (22)$$

The operating point of electrolyzer is constrained within an lower and upper bound, as shown in Eq. (21), where $\underline{\alpha}$ is the lower bound coefficient and R_Z is the power capacity. With the current technologies,

Table 6
Electrolyzer system parameters.

Parameter	Symbol	Value	Unit	Reference
Efficiency	η_Z	60	%	[66]
Conversion factor	PH	360	m^3/MWh	[66]
Min operating point	$\underline{\alpha}$	20	%	
Rated power	R_Z	1.2	MW	[68]
Unit cost	ce	1,500,000	\$/MW	[69]
Maintenance cost	M_Z	$0.02 \cdot C_Z$	\$/year	[70]

Table 7
Storage and tank parameters.

Component	Efficiency	Cost
Battery	$\eta_C = \eta_D = 0.9$	1 M \$/MW for 4-h duration storage [73,74]
Thermal	$\eta_C = \eta_D = 0.85$	622,000 \$/MW [75]
Hydrogen Tank	$\eta_C = \eta_D = 1$	103.75 \$/ m^3 [76]
Water Tank	$\eta_C = \eta_D = 1$	250 \$/ m^3 [77]

the minimum operating point of the electrolyzer is between 10 % and 50 % of its nominal power [36]; therefore, $\underline{\alpha} = 20$ % is used here. The cost of the electrolyzer system, C_Z , can be calculated using Eq. (22), which is the product of the number of units N_Z , the rated power capacity R_Z , and the specific cost ce of the electrolyzer. The relevant parameters of electrolyzer are listed in Table 6.

4.5. Storage and tanks

Storage devices play an crucial role in balancing generation and demand by providing operational flexibility to the energy system. In this study, the storage and tank systems include battery storage, thermal storage, water tank and hydrogen tank, all of which have similar functions and limited capacity. The model operates on an hourly time step, which means that all power values are inherently interpreted as energy over one-hour intervals. The general dynamics of charging and discharging activities for these storage devices, along with the associated constraints, are mathematically formulated in Eqs. (23)–(26) [71,72]. Here, px_t^- and px_t^+ are the discharge and charge amounts, respectively, while px_t is the resulting net amount, which can be positive or negative. The storage or tank level at time t , denoted as s_t , depends on previous charging and discharging activities. R_S is the capacity of the storage or tank, which is a decision variable in capacity planning. The parameters η_C and η_D denote the charge and discharge efficiency of the storage or tank, while δ is the maximum charging or discharging coefficient. The investment cost of storage or tank, C_S , is calculated using Eq. (27) as the product of the rated capacity R_S and the specific cost cs .

$$px_t = px_t^- - px_t^+ \quad (23)$$

$$s_t = s_{t-1} - \frac{px_t^-}{\eta_D} + px_t^+ \cdot \eta_C \quad (24)$$

$$0 \leq s_t \leq R_S \quad (25)$$

$$-R_S \cdot \delta \leq px_t \leq R_S \cdot \delta \quad (26)$$

$$C_S = R_S \cdot cs \quad (27)$$

Here, $\delta = 0.25$ is used for all storages or tanks. The relevant parameters of storages and tanks are listed in Table 7.

4.6. Demand balance

Based on the supply-demand relationships in the system scheme (Fig. 1), the following balance equations can be derived for each type of demand, as shown in Eqs. (28)–(31).

$$wf_t + px_t + \Delta w = Dw_t, \quad (28)$$

Water balance: desalination output, water storage, and slack must equal water demand.

$$qT_t + qB_t + px_t + \Delta q = Dq_t, \quad (29)$$

Heat balance: heat from gas turbine, boiler, thermal storage, and slack must meet heat demand.

$$hf_t + px_t + \Delta h = Dh_t, \quad (30)$$

Hydrogen balance: electrolyzer output, hydrogen storage, and slack must meet hydrogen demand.

$$pR_t + pT_t + px_t - pD_t - pZ_t + \Delta p = Dp_t. \quad (31)$$

Electricity balance: Renewable generation, gas turbine output, and battery discharge must cover electricity demand as well as the electricity consumed by desalination and the electrolyzer.

Here, px_t represents the charging or discharging amount for the specific storage or tank in each respective equation. Dp_t and Dq_t denote the electricity demand and thermal demand, respectively, and Dh_t and Dw_t denote the hydrogen and freshwater demand, respectively.

5. Co-optimization planning model

This paper presents a co-optimization model that aims to minimize the investment cost during the capacity planning stage, as well as the maintenance and operational costs during the subsequent operational stage. The design decision is to determine the capacity sizes of all subsystems within the MRE-MES. Two complementary models are developed to address different levels of uncertainty in system planning: the Deterministic Model and the Two-Stage Stochastic Model.

5.1. Deterministic model

The deterministic model formulates the planning problem under a single fixed trajectory of renewable resource availability and end-use demands. The objective is to minimize the total system investment cost C_{Inv} , system maintenance cost C_{Mtn} and subsequent operational cost C_{Opr} . The system capital cost C_{Inv} is calculated as the sum of capital costs of all sub-energy systems, as shown in Eq. (32). Note that C_S is a general term representing the cost of the four storage systems and tanks. Similarly, in Eq. (33), C_{Mtn} represents the maintenance cost of all sub-energy systems. The operation cost $C_{Opr,t}$ at each time step t consists of two components: natural gas purchase cost (first term) and carbon emission cost (second term), as expressed in Eq. (34). Here, C_e is carbon emission price, F_e is the emission factor of natural gas, and Gp_t is the natural gas purchase price.

$$C_{Inv} = C_W + C_P + C_V + C_D + C_G + C_B + C_Z + C_S \quad (32)$$

$$C_{Mtn} = M_W + M_P + M_V + M_D + M_G + M_B + M_Z + M_S \quad (33)$$

$$C_{Opr,t} = Gp_t \cdot (gT_t + gB_t) + C_e \cdot F_e \cdot (gT_t + gB_t) \quad (34)$$

$$C_{obj} = C_{Inv} \cdot \frac{r \cdot (1+r)^{L_p}}{(1+r)^{L_p} - 1} + \sum_t C_{Opr,t} + C_{Mtn} \quad (35)$$

The final objective function is defined in Eq. (35). To map the lifetime investment into the operational time horizon in one year, an adjusted equated installment factor is used, where L_p is the project lifetime and r is the financial interest rate. The first term in Eq. (35) is the annualized investment cost. In addition, the deterministic framework is used to assess the impact of uncertainty in demand and ambient conditions. Capacities for all subsystems are fixed at the baseline design, and the model is solved repeatedly with randomized input trajectories to evaluate operational robustness and quantify how these perturbations affect the operational cost.

5.2. Two-stage stochastic model

To address future uncertainties in demand and ambient conditions and to make more robust decisions during the capacity planning stage, the deterministic model provided in [Section 5.1](#) is extended to a two-stage stochastic optimization model. In the two-stage stochastic optimization, the first stage represents capacity planning, where investment decisions are made, while the second stage focuses on operations as the recourse stage, adjusting the system to respond to specific scenarios. The objective function of the model is expressed as:

$$C_{obj} = C_{Inv} \cdot \frac{r \cdot (1+r)^{L_p}}{(1+r)^{L_p} - 1} + \sum_{s,t} P_s \cdot C_{Opr,s,t} + C_{Mtn} \quad (36)$$

where P_s represents the probability of scenario s , and $C_{Opr,s,t}$ denotes the operational cost for each scenario s at time t . Additionally, the operational constraints must be revised to incorporate each scenario.

The analysis proceeds under the following modeling assumptions:

- Fuel prices are treated as time-invariant over the simulated year. Natural gas purchases and the associated carbon charge apply only to the gas turbine and auxiliary boiler.
- The capital, and operation and maintenance unit costs are fixed parameters that do not vary over the study horizon.
- Technological advancements and performance drift are not modeled; component efficiencies and unit costs remain constant throughout the analysis.
- No explicit curtailment variables were included. Any surplus renewable generation must be absorbed by storage or flexible conversion loads (e.g., desalination, electrolyzer); otherwise, feasibility is ensured via capacity sizing and hourly dispatch rather than by accounting for an explicit curtailment term.
- All balances and device operations were enforced at an hourly resolution. The power variables were interpreted as hourly averages and integrated as energy with $\Delta t = 1$ h.

6. Case study and scenario setting

In this study, Wilmington, North Carolina, a coastal city in the southeastern United States, was selected as the reference location to demonstrate the flexibility and applicability of the proposed model. This

choice was motivated by the city's geographical and climatic characteristics, which make it representative of coastal communities, where renewable resource variability and infrastructure resilience are critical considerations. The meteorological data used in the simulations were obtained from multiple databases. Wind speed and temperature were collected from the Weather Underground website [78], and solar irradiation was retrieved from the National Solar Radiation Database, which provides high-resolution coverage across more than 1,400 monitoring stations in the United States [79]. For wave energy conversion, wave height data were obtained from the Marine Data Library [80]. All raw datasets were checked for their completeness and quality. The time series were synchronized to an hourly resolution to ensure consistency across resources and demand. To ensure consistency, all meteorological datasets were synchronized for the same time periods, namely, the first week of January, representing typical winter conditions, and the first week of July, representing typical summer conditions. These two periods were chosen to capture seasonal variations, and the resulting profiles are shown in [Fig. 3](#).

The demand data were modeled to represent the hourly profiles of electricity, thermal energy, hydrogen, and freshwater. Electricity and thermal demands were based on reference load profiles for commercial and residential buildings obtained from the Open Energy Information platform [81]. Hydrogen and freshwater demands were derived by the team from existing studies reported in the literature [15,16,82]. [Fig. 2](#) illustrates these demand patterns for the two representative weeks, which were selected to capture typical seasonal variations in energy consumption.

We adopted a representative seasonal approach to balance accuracy and computational feasibility. Simulations were conducted for one winter week and one summer week, with the operational costs obtained from these two periods aggregated and scaled using a 365/14 multiplier to estimate the annual operational cost, as expressed in [Eq. \(35\)](#): Although using a full year of data could provide additional detail, this would dramatically increase the computational burden without yielding proportionate improvements in insight. By considering seasonal characteristics and extracting two representative weeks, this study ensured that both meteorological and demand variabilities were adequately captured while maintaining computational efficiency. This approach provides a

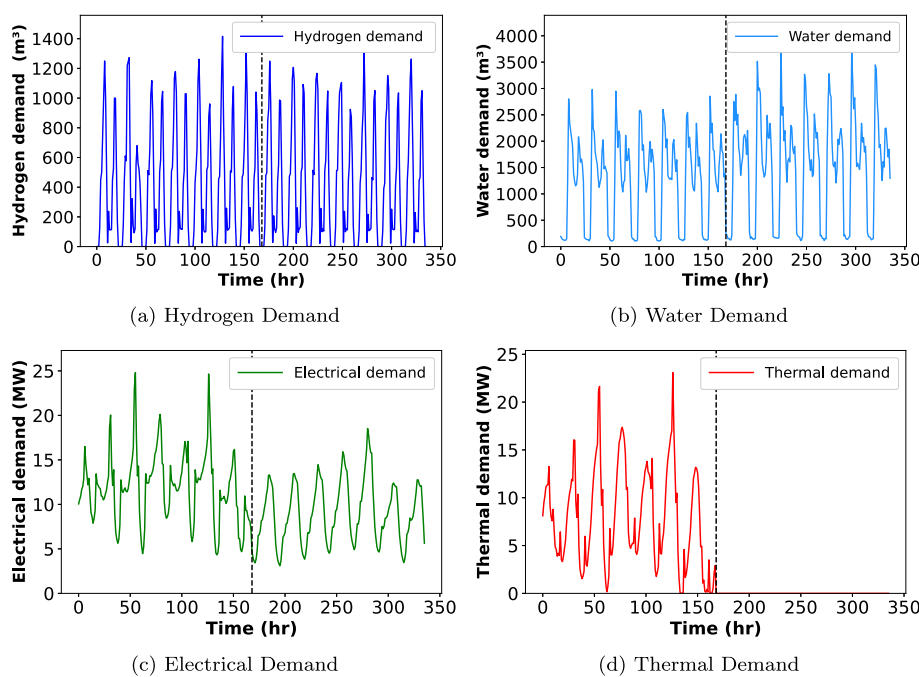


Fig. 2. Various demands (The left side of the dashed line represents typical winter week, while the right side shows typical summer week).

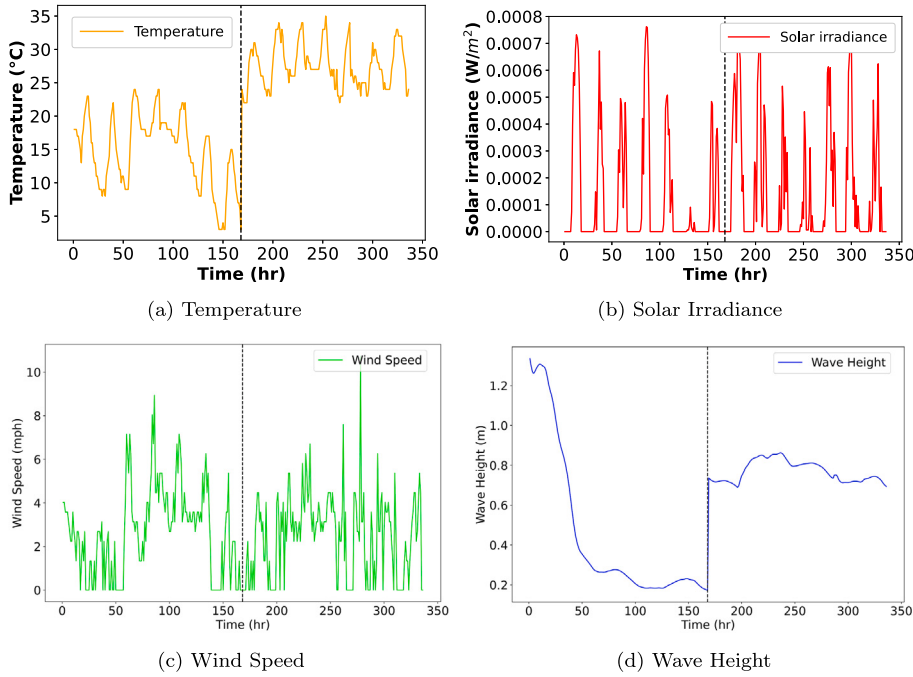


Fig. 3. Environmental and meteorological data (The left side of the dashed line represents typical winter week, while the right side shows typical summer week).

valid and representative foundation for analyzing system performance under diverse seasonal conditions.

In these experiments, two cases are considered in solving the co-optimization model for comparison: 1) Case 1: there are no capacity constraint limitations on maximum available PV array area, water tank capacity and hydrogen storage capacity, 2) Case 2: capacity constraint limitations are considered with a maximum PV array area of 4000 m^2 , maximum water tank capacity of 1000 m^3 , and maximum hydrogen storage capacity of 5000 m^3 . These upper bound limitations are chosen according to the peak water demand and data from [83,84] and the hydrogen storage capacity limit was derived from [85]. The system lifetime and annual interest rate are assumed to be 50 years and 5 %, respectively.

For all experiments, the Gurobi solver (version 11.0.3, supporting non-linear models) is used in a Python environment to solve the proposed non-linear optimization model, with an optimality gap of 0.001. The complete code is available in a public repository.¹

7. Results and discussion

7.1. System configuration with deterministic demand

In this group of experiments, a deterministic case was considered in which the hourly demand profiles and environmental inputs were treated as fixed values without introducing any variability. These profiles represent the baseline operational conditions and were used directly to evaluate the system performance and cost under known demand levels.

For power generation, there are renewable power (RE) sources such as solar, wind, and wave power, as well as power generation from gas turbines in CHP systems. To study the impact of different levels of renewable penetration on the system, the RE power percentage is varied from 0 % to 100 % with 10 % increments, as shown on the x-axis in Fig. 4. In this figure, the left y-axis represents the optimal capacity design

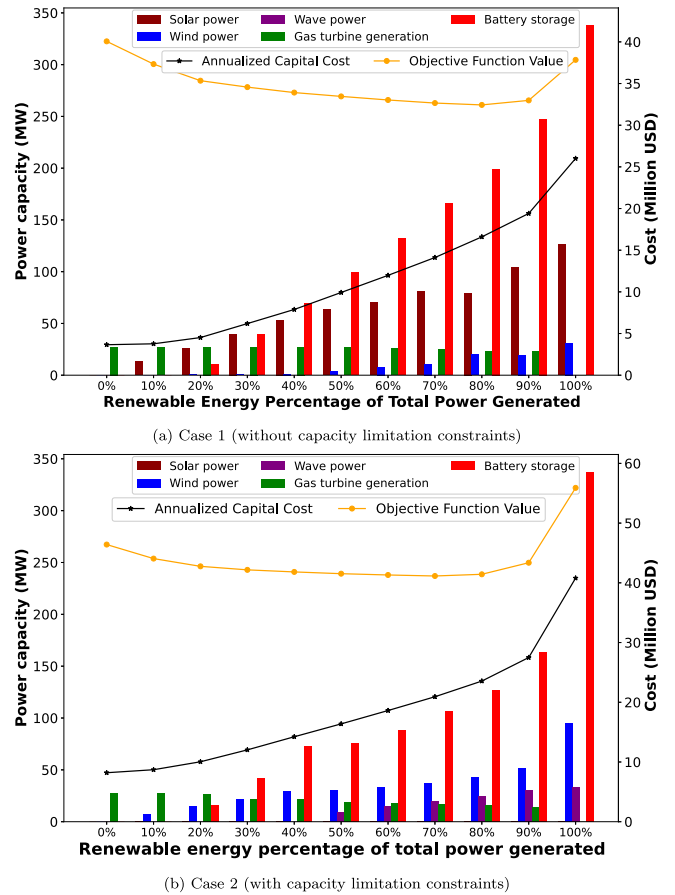


Fig. 4. Impact of increasing renewable energy share on annualized investment costs and power capacity.

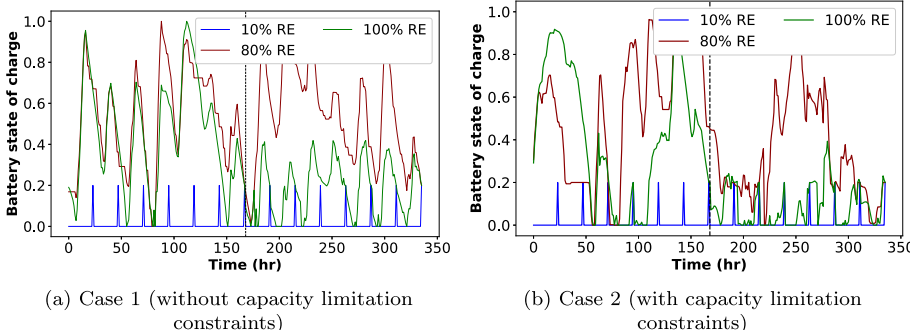
¹ See the repository: <https://github.com/ntduah/MRE-MES-Co-optimization-model>.

Table 8

The capacity decisions of the components and the corresponding costs.

Description	SP (MW)	WTP (MW)	WP (MW)	GTP (MW)	GBP (MW)
0 %RE (Case 1)	0	0	0	27.25	17.33
0 %RE (Case 2)	0	0	0	27.26	17.65
50 % RE (Case 1)	63.20	3.5	0	26.68	17.37
50 % RE (Case 2)	0.62	30	9	19.12	18.99
100 % RE (Case 1)	126.42	31	0	23.09	23.09
100 % RE (Case 2)	0.64	95	0	23.09	23.09
Optimal (Case 1)	78.81	23	0	22	18.36
Optimal (Case 2)	0.8	43.5	13.5	15.94	19.68
Description	BS (MW)	TS (MW)	HS (m³)	WS (m³)	No. Osmosis
0 %RE (Case 1)	0	0	0	37,226	3
0 %RE (Case 2)	0	0	0	0	9
50 % RE (Case 1)	99.46	0	9084	37,226	3
50 % RE (Case 2)	75.24	0	4742	1000	9
100 % RE (Case 1)	337.87	0	28,928	21,394	4
100 % RE (Case 2)	337.31	0	5000	1000	9
Optimal (Case 1)	209.72	0	6451	37,226	3
Optimal (Case 2)	130	0	5000	1000	9
Description	Obj (\$)	ACC (\$)	AOC (\$)	AMC (\$)	No. Electrolyzer
0 %RE (Case 1)	40,064,887	3,656,511	1,349,184	1,233,225	6
0 %RE (Case 2)	46,407,181	8,200,357	1,350,968	2,985,166	6
50 % RE (Case 1)	33,457,648	9,924,752	789,831	2,940,867	6
50 % RE (Case 2)	41,529,275	16,379,205	782,786	4,741,709	5
100 % RE (Case 1)	37,841,510	26,010,893	206,566	6,445,134	4
100 % RE (Case 2)	55,900,947	40,792,974	4,206,566	9,722,491	5
Optimal (Case 1)	32,409,422	17,369,250	408,854	4,380,764	5
Optimal (Case 2)	41,148,316	21,329,147	540,013	5,740,253	5

SP: Solar Power, WTP: Wind Turbine Power, WP: Wave Power, GTP: Gas Turbine Power, GBP: Gas Boiler Power, BS: Battery Storage, TS: Thermal Storage, HS: Hydrogen Storage, WS: Water Storage, Obj: Objective Value, ACC: Annualized Capital Cost, AOC: Annual Operational Cost, AMC: Annual Maintenance Cost.

**Fig. 5.** SOC of the battery storage in two Cases (The left side of the dashed line represents typical winter week, while the right side shows typical summer week).

decisions for different systems, while the right y-axis shows the annualized investment costs and objective function values at different RE penetration levels. For instance, when the RE percentage is set to be 0 % in Case 1 (Fig. 4a), the optimal design capacities for solar, wind, wave, and battery are all 0 MW, while the gas turbine capacity is 27.25 MW (detailed values are in Table 8). When the RE percentage reaches 100 %, the optimal power capacities are 126.42 MW for solar, 31 MW for wind, 0 MW for wave, 23.09 MW for gas turbine, and 337.87 MW for battery. It is observed that the annual investment cost increases as the RE percentage increases, but the total objective function value (including investment, operation, and maintenance costs) decreases for both cases. This is because a higher share of renewable energy reduces operational costs associated with carbon emissions and gas purchases. The objective value reaches its lowest point when the RE percentage is around 80 %. This trade-off between initial capital investment and subsequent long term operation and maintenance costs emphasizes the importance of co-optimization of the two stages. The optimal capacity design decisions for the two cases are also provided in the “Optimal (Case 1)” and “Optimal (Case 2)” rows of Table 8.

The detailed decisions on component sizes and costs are summarized in Table 8. Based on the capacity decisions for solar, wind, and wave energy, it is evident that solar power is more cost-effective compared to wind and wave power. Additionally, in Case 2, where there is a size limitation of 1000 m³ on water storage, the required number of osmosis units reaches a maximum of nine to meet the freshwater demand. The thermal storage capacity is always zero due to its higher cost, as the thermal energy generated by the gas turbine and boiler is sufficient to meet the thermal demand.

Higher RE percentage requires a larger battery capacity to store the variable renewable energy, as shown in Fig. 4. However, the utilization of this capacity varies significantly. As seen from the battery state of charge (SOC) in Fig. 5, the SOC level remains below 40 % for most of the time in the two cases when the system relies on 100 % renewable energy, making it inefficient.

7.2. System configuration with varying demand

In this analysis, we use a Monte Carlo approach to evaluate the impact of uncertainties in various demands and ambient

conditions. Solar irradiation, wind speed, and temperature are assumed to fluctuate within a set range of $\pm 5\%$, using Fig. 3 as the baseline reference. Meanwhile, electricity, hydrogen, water, and thermal loads are perturbed by $\pm 5\%$, $\pm 10\%$, $\pm 15\%$, $\pm 20\%$, and $\pm 25\%$.

and $\pm 25\%$ of the baseline demand from Fig. 2. Using these sampled variations, the deterministic model was executed 200 times to account for variability and assess the impact on capacity design decisions.

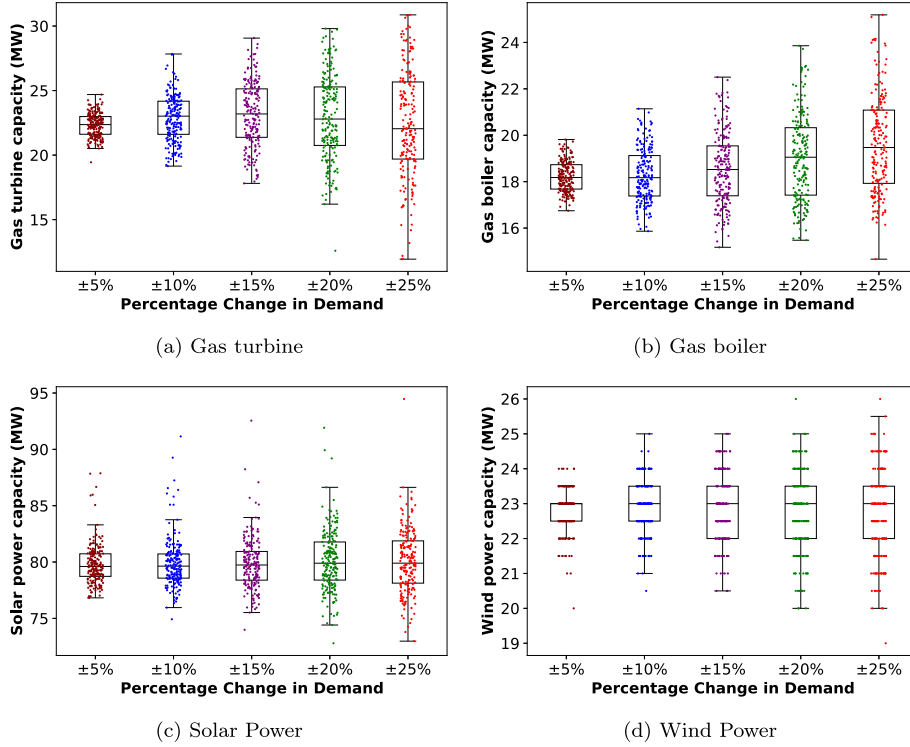


Fig. 6. Distribution of system component capacity with different demand randomness levels in Case 1 (without capacity limitation constraints).

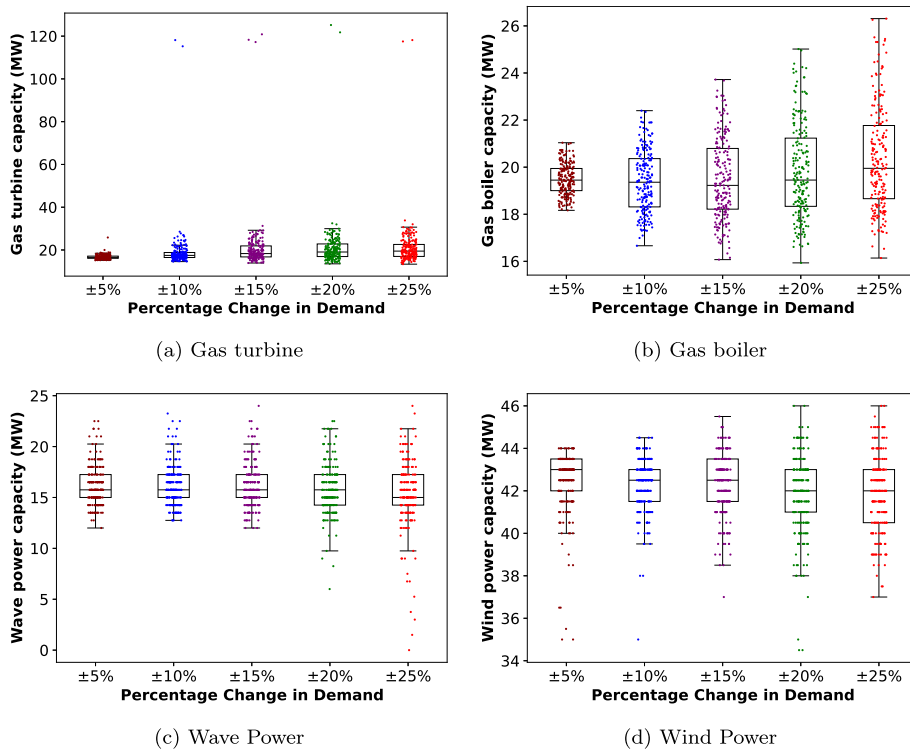


Fig. 7. Distribution of system component capacity with different demand randomness levels in Case 2 (with capacity limitation constraints).

Table 9

System component capacity statistics with different demand randomness levels.

Case 1 (without capacity limitation constraints)												
	SP (MW)			GTP (MW)			GBP (MW)			WTP(MW)		
	$\pm 5\%$	$\pm 15\%$	$\pm 25\%$	$\pm 5\%$	$\pm 15\%$	$\pm 25\%$	$\pm 5\%$	$\pm 15\%$	$\pm 25\%$	$\pm 5\%$	$\pm 15\%$	$\pm 25\%$
Max	87.87	91.15	94.47	24.69	29.06	30.87	19.82	22.51	25.19	24	25	26
Mean	79.82	79.87	80.06	22.33	23.16	22.44	18.22	18.58	19.59	22.80	22.85	22.71
Min	76.82	73.99	72.98	19.44	17.81	11.94	16.75	15.17	14.66	20	20.5	19
WP (MW)			No. Electrolyzer			No. Osmosis			—			
$\pm 5\%$	$\pm 15\%$	$\pm 25\%$	$\pm 5\%$	$\pm 15\%$	$\pm 25\%$	$\pm 5\%$	$\pm 15\%$	$\pm 25\%$	$\pm 5\%$	$\pm 15\%$	$\pm 25\%$	
Max	0	0	0	6	6	6	4	4	4	—	—	—
Mean	0	0	0	5	5	5	3	3	3	—	—	—
Min	0	0	0	5	5	5	3	3	3	—	—	—
BS (MW)			TS (MW)			HS (m ³)			WS(m ³)			
$\pm 5\%$	$\pm 15\%$	$\pm 25\%$	$\pm 5\%$	$\pm 15\%$	$\pm 25\%$	$\pm 5\%$	$\pm 15\%$	$\pm 25\%$	$\pm 5\%$	$\pm 15\%$	$\pm 25\%$	
Max	222.98	227.25	233.61	0	0	0	9905	10,403	14,584	38,698	41,753	43,230
Mean	209.72	209.67	209.36	0	0	0	8040	8246	8337	28,388	23,555	21,837
Min	194.37	191.62	184.99	0	0	0	5055	5398	4838	7972	6763	7328
Case 2 (with capacity limitation constraints)												
	SP (MW)			GTP (MW)			GBP (MW)			WTP (MW)		
	$\pm 5\%$	$\pm 15\%$	$\pm 25\%$	$\pm 5\%$	$\pm 15\%$	$\pm 25\%$	$\pm 5\%$	$\pm 15\%$	$\pm 25\%$	$\pm 5\%$	$\pm 15\%$	$\pm 25\%$
Max	0.80	0.80	0.80	15.17	120.85	118.15	21.04	23.72	26.31	44	45.5	46
Mean	0.78	0.79	0.79	16.72	20.94	21.30	19.49	19.48	20.34	42.41	42.26	41.84
Min	0.25	0.27	0.61	15.17	13.9	13.37	18.17	16.07	16.14	35	37	37
WP (MW)			No. Electrolyzer			No. Osmosis			—			
$\pm 5\%$	$\pm 15\%$	$\pm 25\%$	$\pm 5\%$	$\pm 15\%$	$\pm 25\%$	$\pm 5\%$	$\pm 15\%$	$\pm 25\%$	$\pm 5\%$	$\pm 15\%$	$\pm 25\%$	
Max	22.5	24	24	6	6	6	9	10	11	—	—	—
Mean	16.15	16.12	15.35	5	5	5	8	8	8	—	—	—
Min	12	12	0	5	5	5	8	8	8	—	—	—
BS (MW)			TS (MW)			HS (m ³)			WS(m ³)			
$\pm 5\%$	$\pm 15\%$	$\pm 25\%$	$\pm 5\%$	$\pm 15\%$	$\pm 25\%$	$\pm 5\%$	$\pm 15\%$	$\pm 25\%$	$\pm 5\%$	$\pm 15\%$	$\pm 25\%$	
Max	134.44	140.04	145.50	0	0	0	5000	5000	5000	1000	1000	1000
Mean	122.61	121.73	121.74	0	0	0	4991	4992	4977	1000	1000	1000
Min	94.44	93.81	89.98	0	0	0	4255	4195	4260	1000	1000	1000

SP: Solar Power, WTP: Wind Turbine Power, WP: Wave Power, GTP: Gas Turbine Power, GBP: Gas Boiler Power, BS: Battery Storage, TS: Thermal Storage, HS: Hydrogen Storage, WS: Water Storage.

Figs. 6 and 7 present dot-box plots showing the distribution of the 200 capacity decisions for Case 1 (without capacity limitation constraints) and Case 2 (with capacity limitation constraints), respectively. Table 9 provides detailed values for the maximum, mean, and minimum of the 200 runs. The distribution of capacity decisions demonstrates the varying impacts of different demand randomness levels. Comparing Figs. 6 and 7, we observe distinct patterns with increasing randomness. In Case 1, the maximum values generally increase while the minimum values decrease, leading to a larger range between extremes. In Case 2, however, the minimum values for gas turbine and gas boiler capacities remain relatively stable, even as the maximum values increase. On the other hand, the maximum values for wave power and wind power remain stable. Since the capacities of wave power and wind power depend on the discrete number of wave energy converters and wind turbines, the capacity decisions are presented in a banded pattern. Wave power is not selected in Case 1, indicating that it lacks economic competitiveness compared to other renewable energy options.

When capacity limitations are imposed, the energy mix shifts from being solar- and wind-dominated to wind- and wave-dominated. Solar power generation consistently reaches the upper limit of its allowed capacity across all scenarios. To compensate for the reduced Photovoltaic (PV) capacity, the system increases the use of wave, wind, and gas turbine power, with a significant boost in gas turbine capacity driven by economic factors and its role in maintaining system stability. This

highlights the need for further research and investment to improve the economic viability of wave energy technology. Interestingly, the number of electrolyzers shows minimal variation across all uncertainty levels under both cases, suggesting that the optimal capacity of this component is robust to demand fluctuations. Desalination capacity, represented by osmosis units, exhibits some variability and uncertainty. In Case 1, the average number of osmosis units remains three, with an upper limit of four across all uncertainty levels. In the Case 2, however, the number of osmosis units increases to around nine due to the capacity limits imposed on water storage.

Fig. 8 and Table 10 illustrate that increasing demand uncertainty leads to higher objective function costs for both cases. The constrained case consistently results in higher objective values, largely due to the inclusion of wave power and the reduction in PV capacity. For instance, with a 25 % demand variation, the average objective function cost increases from \$32,585,096.62 in the unconstrained case to \$41,486,699.71 in the constrained scenario, representing a 27 % increase. This notable cost difference underscores the economic impact of certain capacity or practical limitations (e.g., available land, available gas pipeline) on selecting the optimal energy mix.

The Monte Carlo simulation results indicate that system configuration can be significantly influenced by variations in demand. This variability highlights the importance of accounting for uncertainty during the system planning stage to ensure more robust decision-making.

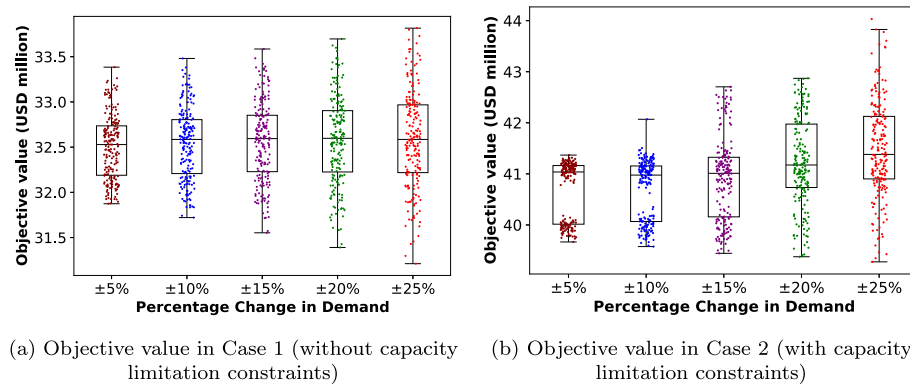


Fig. 8. Objective value distribution with different demand randomness levels.

Table 10

Objective value (in \$) statistics with different demand randomness levels.

Case 1 (without capacity limitation constraints)					
	±5 %	±10 %	±15 %	±20 %	±25 %
Max	33,384,492.78	33,480,754.88	33,585,332.26	33,696,707.96	33,815,711.24
Mean	32,503,833.88	32,539,206.39	32,562,411.90	32,574,774.68	32,585,096.62
Min	31,874,161.94	31,721,900.09	31,552,694.86	31,390,408.95	31,211,235.94
Case 2 (with capacity limitation constraints)					
	41,367,822.88	42,068,725.96	42,704,267.06	42,870,458.57	44,031,102.88
Max	40,710,272.47	40,696,317.99	40,914,914.48	41,228,014.98	41,486,699.71
Mean	39,666,847.05	39,576,291.97	39,443,955.32	39,377,344.59	39,277,194.45

Table 11

Component capacity decisions from two-stage stochastic optimization.

Randomness	PV (MW)	GTP (MW)	GBP (MW)	WTP (MW)	WP (MW)
±5 % (Case 1)	82.12	25.44	18.78	22.5	0
±5 % (Case 2)	0.8	18.34	20.24	42.5	15.75
±25 % (Case 1)	84.63	32.3	21.89	21.5	0
±25 % (Case 2)	0.78	30.37	22.02	40	18.75
Randomness	BS (MW)	TS (MW)	HS (m³)	WS (m³)	No. Electrolyzer
±5 % (Case 1)	219.62	0	8031	9358	5
±5 % (Case 2)	128.51	0	5000	1000	6
±25 % (Case 1)	227.37	0	8251	12,296	5
±25 % (Case 2)	125.94	0	4281	1000	4
Randomness	No. Osmosis	Obj (\$)	EVPI (\$)	—	—
±5 % (Case 1)	4	33,257,398.12	753,564.24	—	—
±5 % (Case 2)	9	41,276,689.20	566,416.73	—	—
±25 % (Case 1)	4	33,635,541.79	1,050,445.16	—	—
±25 % (Case 2)	10	42,959,167.65	1,472,467.93	—	—

SP: Solar Power, WTP: Wind Turbine Power, WP: Wave Power, GTP: Gas Turbine Power, GBP: Gas Boiler Power, BS: Battery Storage, TS: Thermal Storage, HS: Hydrogen Storage, WS: Water Storage. EVPI: Expected Value of Perfect Information.

7.3. System configuration with two-stage stochastic optimization

In this study, a two-stage stochastic optimization model was developed to improve the robustness of system planning under uncertainty. A total of 25 scenarios were generated to represent possible future states, each reflecting stochastic variations in both energy demand and environmental conditions. Specifically, solar irradiation, wind speed, and temperature were assumed to fluctuate within a set range of ±5 %. Similarly, electricity, hydrogen, water, and thermal loads were perturbed by ±5 % and ±25 %. To maintain generality, the random variables were assumed to follow a uniform distribution and were treated as independent. The number of scenarios was chosen to provide a reasonable trade-off between the model accuracy and computational efficiency. For each scenario, the model simultaneously optimizes capacity

planning and operational decisions. Although 25 scenarios were used in this study, the framework can accommodate more scenarios if needed, with scenario reduction techniques available to manage computational complexity.

The optimal capacity decisions for each component are summarized in Table 11. With greater uncertainty in demand, the objective value increases, reflecting the system's response to higher levels of variability. In Case 2 (with capacity limitation constraints), the gas turbine capacity significantly increased to handle future uncertainties as the randomness level rose from 5 % to 25 %. For instance, under a 25 % randomness level (Case 2), the optimal objective value obtained through the two-stage stochastic optimization is \$42,959,167.65, which is \$1,071,935.23 lower than the worst-case (maximum) value of \$44,031,102.88 under

the same conditions, as reported in [Table 10](#). This substantial difference demonstrates the benefits of incorporating stochastic optimization, resulting in a more robust decision that effectively mitigates the risks posed by future uncertain demand conditions.

To evaluate the potential worth of more accurate forecasts, the Expected Value of Perfect Information (EVPI) is calculated, as shown in [Table 11](#). The EVPI quantifies how much better off a decision-maker could be if they had perfect knowledge about uncertain parameters. The EVPI is calculated as $EVPI = SP - WS$, where SP represents the objective value obtained from stochastic model. Meanwhile, WS is the expected value of the optimal decision that could be made given perfect information. WS is the mean value in [Table 10](#). As shown, EVPI is higher when the level of randomness is high.

8. Conclusions

The integration of marine renewable energy with a multi-energy system offers a promising pathway to addressing the diverse energy needs of expanding coastal communities while promoting environmental sustainability and resilience. Unlike prior studies, this study develops a generalized, flexible MRE-MES framework that jointly optimizes capital and operational costs for coastal communities. Through a two-stage stochastic optimization approach, the model effectively mitigates the impacts of uncertainties in demand and renewable energy availability, resulting in a more robust capacity design. Specifically, in scenarios with 25 % demand variability, the two-stage stochastic optimization reduced costs by approximately \$1 million compared to the deterministic worst-case scenario, demonstrating the value of considering uncertainties in planning. Moreover, the results indicate that a balanced integration of renewable sources—wind, wave, and solar—leads to lower operational costs and improved system efficiency, particularly when capacity constraints are in place. The results demonstrate that the stochastic model significantly improves the system robustness, effectively managing fluctuations without substantial overdesign. It also achieves a better trade-off between investment and operational performance, particularly under high-uncertainty conditions. The generalized nature of this framework allows for easy adaptation to different coastal contexts, whether small- or large-scale, depending on local renewable resource availability, infrastructure limitations, and community needs.

Although the proposed MRE-MES framework is designed to be general and adaptable, its validation is limited by a conceptual case study using only two representative weeks rather than a full-year-long simulation. While these weeks highlight seasonal contrasts, they fail to capture the full temporal variability required for robust investment planning. The economic analyses also overlook component degradation, replacement cycles, and life-cycle and fuel cost fluctuations. However, these simplifications support computational feasibility and model applicability. Future studies should address these gaps by including a wider range of technologies, such as heat pumps, conducting full-year simulations, and adopting comprehensive life-cycle cost analyses. Incorporating predictive control and AI-driven energy management could also improve responsiveness to uncertainty, enabling more dynamic and cost-effective operations.

Nevertheless, the proposed system framework offers valuable guidance to planners and policymakers aiming to develop sustainable and resilient energy solutions in coastal regions. Solar and wind energy remain the most cost-effective resources, while wave energy adoption is still constrained by current costs and will require targeted incentives and further cost reductions. Early stage research and pilot projects should be supported through incentives such as grants, tax credits, or procurement guarantees, especially in areas with untapped offshore resources. Integrated energy planning frameworks that co-optimize multiple energy vectors should replace siloed approaches to improve efficiency, reduce redundancies, and enhance flexibility. Regulatory agencies should require the use of site-specific data and scenario-based

planning for marine renewable and multi-energy systems, as coastal areas vary widely in terms of their conditions and constraints.

CRediT authorship contribution statement

Nana Duah: Writing – original draft, Software, Investigation. **Yang Chen:** Writing – review & editing, Supervision, Methodology, Funding acquisition, Conceptualization. **Om Prakash Yadav:** Writing – review & editing, Project administration, Funding acquisition. **Jun Chen:** Writing – review & editing, Resources, Funding acquisition.

Declaration of competing interest

The authors declare that they have no known competing financial interests or personal relationships that could have appeared to influence the work reported in this paper.

Acknowledgment

The authors gratefully acknowledge the financial support provided by the North Carolina Renewable Ocean Energy Program of the Coastal Studies Institute from 2023–2024.

Data availability

Data will be made available on request.

References

- [1] H. Mathew, S. Kyle, S. Daniel, Research note: demographic change on the United States coast, 2020–2100, *Demography* 59 (2022) 1221–1232, <https://doi.org/10.1215/00703370-10127418>
- [2] R. Manasseh, S.A. Sannasiraj, K.L. McInnes, V. Sundar, P. Jalilah, Integration of wave energy and other marine renewable energy sources with the needs of coastal societies, *Int. J. Ocean Clim. Syst.* 8 (1) (2017) 19–36, <https://doi.org/10.1177/1759313116683962>
- [3] D. Groppi, S.K.P. Kannan, F. Gardumi, D.A. Garcia, Optimal planning of energy and water systems of a small island with a hourly OSeMOSYS model, *Energy Convers. Manag.* 276 (2023) 116541, <https://doi.org/10.1016/j.enconman.2022.116541>
- [4] K. Kazimierczuk, C. Henderson, K. Duffy, S. Hanif, S. Bhattacharya, S. Biswas, E. Jacroux, D. Prezioso, D. Wu, D. Bhattacharya, et al., A socio-technical assessment of marine renewable energy potential in coastal communities, *Energy Res. Soc. Sci.* 100 (2023) 103098, <https://doi.org/10.1016/j.erss.2023.103098>
- [5] X. Liguo, M. Ahmad, S.I. Khattak, Impact of innovation in marine energy generation, distribution, or transmission-related technologies on carbon dioxide emissions in the United States, *Renew. Sustain. Energy Rev.* 159 (2022) 112225, <https://doi.org/10.1016/j.rser.2022.112225>
- [6] B. Nikonorow, Powered by the moon: the tantalizing potential of marine energy to power communities in the short and long terms, *SSRN*, 2023, <https://doi.org/10.2139/ssrn.4473958>
- [7] European Commission, Marine renewable energy, Available at https://blue-economy-observatory.ec.europa.eu/eu-blue-economy-sectors/marine-renewable-energy_en.
- [8] US Energy Information Administration, Waves have a lot of energy, 2023, Available at <https://www.eia.gov/energyexplained/hydropower/wave-power.php>.
- [9] S. Rehman, L.M. Alheims, M.M. Alam, L. Wang, Z. Toor, A review of energy extraction from wind and ocean: technologies, merits, efficiencies, and cost, *Ocean Eng.* 267 (2023) 113192, <https://doi.org/10.1016/j.oceaneng.2022.113192>
- [10] V. Smil, *Power Density: A Key to Understanding Energy Sources and Uses*, MIT Press, 2015.
- [11] J.O. Dabiri, J.R. Greer, J.R. Koseff, P. Moin, J. Peng, A new approach to wind energy: opportunities and challenges, *Phys. Sustain. Energy III Using Energy Effic. Prod. Renewably* 1652 (1) (2015) 51–57.
- [12] Y. Du, Y. Men, X. Lu, J. Liu, F. Qiu, B. Chen, Coastal community resiliency enhancement using marine hydrokinetic (MHK) resources and networked microgrids, 2020, Available at <https://publications.anl.gov/anlpubs/2021/02/165365.pdf>.
- [13] X. Wu, J. Liu, Y. Men, B. Chen, X. Lu, Optimal energy storage system and smart switch placement in dynamic microgrids with applications to marine energy integration, *IEEE Trans. Sustain. Energy* 14 (2) (2022) 1205–1216, <https://doi.org/10.1109/TSTE.2022.3226116>
- [14] M.D. Caballero, T. Gunda, Y.J. McDonald, Energy justice & coastal communities: the case for meaningful marine renewable energy development, *Renew. Sustain. Energy Rev.* 184 (2023) 113491.
- [15] Y. Chen, J. Chen, C. Liu, G. Liu, M. Ferrari, A. Sundararajan, Integrated modeling and optimal operation of multi-energy system for coastal community, in: 2023 IEEE International Conference on Electro Information Technology (eIT), IEEE, 2023, pp. 211–216, <https://doi.org/10.1109/eIT57321.2023.10187307>
- [16] M. Jalili, M. Sedighizadeh, A.S. Fini, Optimal operation of the coastal energy hub considering seawater desalination and compressed air energy storage system, *Therm. Sci. Eng. Prog.* 25 (2021) 101020, <https://doi.org/10.1016/j.tsep.2021.101020>

- [17] K. MacManus, D. Balk, H. Engin, G. McGranahan, R. Inman, Estimating population and urban areas at risk of coastal hazards, 1990–2015: how data choices matter, *Earth Syst. Sci. Data* 13 (12) (2021) 5747–5801, <https://doi.org/10.5194/essd-13-5747-2021>
- [18] S.A. Hemmerling, C. DeMyers, J. Parfait, E. Piñero, M.M. Baustian, M. Bregman, D. Di Leonardo, C. Esposito, I.Y. Georgiou, A. Grismore, et al., A community-informed transdisciplinary approach to coastal restoration planning: maximizing the social and ecological co-benefits of wetland creation in Port Fourchon, Louisiana, USA, *Front. Environ. Sci.* 11 (2023) 235, <https://doi.org/10.3389/fenvs.2023.1105671>
- [19] J. Ariyama, G.F.S. Boisramé, M.R. Brand, Water budgets for the delta watershed: putting together the many disparate pieces, San. Franc. Estuary Watershed Sci. 17 (2) (2019) <https://doi.org/10.15447/sfews.2019v17iss2art3>
- [20] B. Bajema, N. Britton, J. Hezir, M. Kenderdine, A. Maranville, M. Schomburg, E. Gençer, The U.S. hydrogen demand action plan, 2023, <https://efifoundation.org/wp-content/uploads/sites/3/2023/02/EFI-Hydrogen-Hubs-FINAL-2.1.pdf>.
- [21] U.S. Department of Energy, U.S. national clean hydrogen strategy and roadmap, 2023, https://www.hydrogen.energy.gov/docs/hydrogenprogramlibraries/pdfs/us-national-clean-hydrogen-strategy-roadmap.pdf?sfvrsn=c425b44f_5.
- [22] A. Aktas, Y. Kirçek, A novel optimal energy management strategy for off-shore wind/marine current/battery/ultracapacitor hybrid renewable energy system, *Energy* 199 (2020) 117425, <https://doi.org/10.1016/j.energy.2020.117425>
- [23] S.M. Ezzati, H. Mohammadnezhad Shourkaei, F. Faghhihi, S. Soleymani, S.B. Mozafari, Emission based economic dispatch in the context of energy hub concept considering tidal power plants, *J. Energy Manag. Technol.* 4 (3) (2020) 15–22, <https://doi.org/10.22109/JEMT.2020.204349.1202>
- [24] M. Javidsharifi, T. Niknam, J. Aghaei, G. Mokryani, Multi-objective short-term scheduling of a renewable-based microgrid in the presence of tidal resources and storage devices, *Appl. Energy* 216 (2018) 367–381, <https://doi.org/10.1016/j.apenergy.2017.12.119>
- [25] N. Faridnia, D. Habibi, S. Lachowicz, A. Kavousifard, Optimal scheduling in a microgrid with a tidal generation, *Energy* 171 (2019) 435–443, <https://doi.org/10.1016/j.energy.2018.12.079>
- [26] T. Dillon, B. Maurer, M. Lawson, B. Polagye, Forecast-based stochastic optimization for a load powered by wave energy, *Renew. Energy* 226 (2024) 120330, <https://doi.org/10.1016/j.renene.2024.120330>
- [27] G. Ceusters, R.C. Rodríguez, A.B. García, R. Franke, G. Deconinck, L. Helsen, A. Nowé, M. Messagie, L.R. Camargo, Model-predictive control and reinforcement learning in multi-energy system case studies, *Appl. Energy* 303 (2021) 117634.
- [28] A. Parwal, M. Fregelius, I. Temiz, M. Göteman, J.G. de Oliveira, C. Boström, M. Leijon, Energy management for a grid-connected wave energy park through a hybrid energy storage system, *Appl. Energy* 231 (2018) 399–411, <https://doi.org/10.1016/j.apenergy.2018.09.146>
- [29] M. Nazari-Heris, F. Jabari, B. Mohammadi-Ivatloo, S. Asadi, M. Habibnezhad, An updated review on multi-carrier energy systems with electricity, gas, and water energy sources, *J. Clean. Prod.* 275 (2020) 123136, <https://doi.org/10.1016/j.jclepro.2020.123136>
- [30] N. Li, X. Zhao, X. Shi, Z. Pei, H. Mu, F. Taghizadeh-Hesary, Integrated energy systems with cchp and hydrogen supply: a new outlet for curtailed wind power, *Appl. Energy* 303 (2021) 117619, <https://doi.org/10.1016/j.apenergy.2021.117619>
- [31] D. Wen, M. Aziz, Data-driven energy management system for flexible operation of hydrogen/ammonia-based energy hub: a deep reinforcement learning approach, *Energy Convers. Manag.* 291 (2023) 117323, <https://doi.org/10.1016/j.enconman.2023.117323>
- [32] A. Franzoso, G. Fambri, M. Badami, Deep reinforcement learning as a tool for the analysis and optimization of energy flows in multi-energy systems, *Energy Convers. Manag.* 341 (2025) 120095.
- [33] F. Jalilian, M.A. Mirzaei, K. Zare, B. Mohammadi-Ivatloo, M. Marzband, A. Anvari-Moghaddam, Multi-energy microgrids: an optimal despatch model for water-energy nexus, *Sustain. Cities Soc.* 77 (2022) 103573, <https://doi.org/10.1016/j.scs.2021.103573>
- [34] Y. Chen, M. Hu, Z. O'Neill, A collaborative decision model for low energy building design optimization, in: International Design Engineering Technical Conferences and Computers and Information in Engineering Conference, vol. 57175, American Society of Mechanical Engineers, 2015, p. V007T06A025. <https://doi.org/10.1115/DETC2015-47288>
- [35] A. Azad, H. Shateri, Design and optimization of an entirely hybrid renewable energy system (wt/pv/bw/hs/tes/evpl) to supply electrical and thermal loads with considering uncertainties in generation and consumption, *Appl. Energy* 336 (2023) 120782, <https://doi.org/10.1016/j.apenergy.2023.120782>
- [36] N.S. Attemene, K.S. Agbli, S. Fofana, D. Hissel, Optimal sizing of a wind, fuel cell, electrolyzer, battery and supercapacitor system for off-grid applications, *Int. J. Hydrog. Energy* 45 (8) (2020) 5512–5525, <https://doi.org/10.1016/j.ijhydene.2019.05.212>
- [37] M.H. Jahangir, S. Fakouriyan, M.A. Vaziri Rad, H. Dehghan, Feasibility study of on/off grid large-scale pv/wt/wecc hybrid energy system in coastal cities: a case-based research, *Renew. Energy* 162 (2020) 2075–2095, <https://doi.org/10.1016/j.renene.2020.09.131>
- [38] M. Temiz, I. Dincer, Development and assessment of an onshore wind and concentrated solar based power, heat, cooling and hydrogen energy system for remote communities, *J. Clean. Prod.* 374 (2022) 134067, <https://doi.org/10.1016/j.jclepro.2022.134067>
- [39] Z. Wang, A. Xuan, X. Shen, Y. Du, H. Sun, A robust planning model for offshore microgrid considering tidal power and desalination, *Appl. Energy* 350 (2023) 121713, <https://doi.org/10.1016/j.apenergy.2023.121713>
- [40] H. Bahlawan, M. Morini, M. Pinelli, P.R. Spina, M. Venturini, Simultaneous optimization of the design and operation of multi-generation energy systems based on life cycle energy and economic assessment, *Energy Convers. Manag.* 249 (2021) 114883, <https://doi.org/10.1016/j.enconman.2021.114883>
- [41] Y. He, S. Guo, J. Zhou, J. Ye, J. Huang, K. Zheng, X. Du, Multi-objective planning-operation co-optimization of renewable energy system with hybrid energy storages, *Renew. Energy* 184 (2022) 776–790, <https://doi.org/10.1016/j.renene.2021.11.116>
- [42] L. Liu, R. Zhai, Y. Hu, Multi-objective optimization with advanced exergy analysis of a wind-solar-hydrogen multi-energy supply system, *Appl. Energy* 348 (2023) 121512, <https://doi.org/10.1016/j.apenergy.2023.121512>
- [43] Q. Ma, X. Huang, F. Wang, C. Xu, R. Babaei, H. Ahmadian, Optimal sizing and feasibility analysis of grid-isolated renewable hybrid microgrids: effects of energy management controllers, *Energy* 240 (2022) 122503, <https://doi.org/10.1016/j.energy.2021.122503>
- [44] Wind turbine cost: worth the million-dollar price in 2022?, 2024, Available at <https://weatherguardwind.com/how-much-does-wind-turbine-cost-worth-it/>.
- [45] S. Tyler, D. Patrick, M. Daniel, 2022 cost of wind energy review, 2023, Available at <https://www.nrel.gov/docs/fy24osti/88335.pdf>.
- [46] Aeronautica 500kw wind turbine, Available at <https://www.aeronauticawind.com/aeronautica-500kw>.
- [47] IRENA, Renewable power generation costs in 2022, international renewable energy agency, Abu Dhabi, 2023, Available at <https://www.irena.org/Publications/2023/Aug/Renewable-Power-Generation-Costs-in-2022>.
- [48] R. Hammond, A. Cooperman, Windfarm operations and maintenance cost-benefit analysis tool (wombat), 2023, Available at <https://www.nrel.gov/docs/fy23osti/83712.pdf>.
- [49] Z. Song, C.L. McElvany, A.B. Phillips, I. Celik, P.W. Krantz, S.C. Watthage, G.K. Liyanage, D. Apul, M.J. Heben, A techno-economic analysis of perovskite solar module manufacturing with low-cost materials and techniques, *Energy Environ. Sci.* 10 (6) (2017) 1297–1305, <https://doi.org/10.1039/C7EE00757D>
- [50] Rajib Hasan, Recent operation and maintenance cost of solar power plant, <https://openread.net/operation-and-maintenance-cost-of-solar-power-plant/> (Accessed 2025-Jul-28).
- [51] A. Walker, J. Desai, Understanding solar photovoltaic system performance: an assessment of 75 federal photovoltaic systems, Tech. Rep. DOE/GO-102021-5627, U.S. Department of Energy, Federal Energy Management Program, 2021. <https://www.energy.gov/sites/default/files/2022-02/understanding-solar-photovoltaic-system-performance.pdf> (Accessed 2025-Aug-4).
- [52] AQ Energy, How efficient are commercial solar panels? find out now, 2025 <https://www.aq.energy/blog/commercial-solar-panel-efficiency> (accessed: 2025-Jul-28).
- [53] M. Özger, A. Altunkaynak, Z. Sen, Stochastic wave energy calculation formulation, *Renew. Energy* 29 (10) (2004) 1747–1756, <https://doi.org/10.1016/j.renene.2004.01.009>
- [54] W. Sheng, H. Li, A method for energy and resource assessment of waves in finite water depths, *Energies* 10 (4) (2017) 460, Multidisciplinary Digital Publishing Institute. <https://doi.org/10.3390/en10040460>
- [55] A. Babarit, A database of capture width ratio of wave energy converters, *Renew. Energy* 80 (2015) 610–628, <https://doi.org/10.1016/j.renene.2015.02.049>
- [56] M.H. Jahangir, R. Alimohamadi, M. Montazeri, Performance comparison of pelamis, wavestar, langley, oscillating water column and aqua buoy wave energy converters supplying islands energy demands, *Energy Rep.* 9 (2023) 5111–5124, <https://doi.org/10.1016/j.egyr.2023.04.051>
- [57] H. Boughrim, A. El Marjani, R. Nechad, I. Hajjout, Ocean wave energy conversion: a review, *J. Mar. Sci. Eng.* 12 (11) (2024) 1922.
- [58] C. Guo, W. Sheng, D.G. De Silva, G. Aggidis, A review of the leveled cost of wave energy based on a techno-economic model, *Energies* 16 (5) (2023) 2144, <https://doi.org/10.3390/en16052144>
- [59] B. Cyprien, R. Sandeep, K. Jens, Cost analysis of wave energy in the Pacific, 2015, Available at https://wacop.gsd.spc.int/WACOP-COE_Wave_Pacific-FINAL.pdf.
- [60] P. Cabrera, M. Folley, J.A. Carta, Design and performance simulation comparison of a wave energy-powered and wind-powered modular desalination system, *Desalination* 514 (2021) 115173, <https://doi.org/10.1016/j.desal.2021.115173>
- [61] M.M. Generous, N.A.A. Qasem, U.A. Akbar, S.M. Zubair, Techno-economic assessment of electrodialysis and reverse osmosis desalination plants, *Sep. Purif. Technol.* 272 (2021) 118875, <https://doi.org/10.1016/j.seppur.2021.118875>
- [62] M. Jadidbonab, S. Madadi, B. Mohammadi-Ivatloo, Hybrid strategy for optimal scheduling of renewable integrated energy hub based on stochastic/robust approach, *J. Energy Manag. Technol.* 2 (4) (2018) 29–38, <https://doi.org/10.22109/JEMT.2018.142275.1113>
- [63] Z. Liu, Y. Chen, R. Zhuo, H. Jia, Energy storage capacity optimization for autonomy microgrid considering CHP and EV scheduling, *Appl. Energy* 210 (2018) 1113–1125, <https://doi.org/10.1016/j.apenergy.2017.07.002>
- [64] A.V. Olympios, A.M. Pantaleo, P. Sapin, C.N. Markides, On the value of combined heat and power (chp) systems and heat pumps in centralised and distributed heating systems: lessons from multi-fidelity modelling approaches, *Appl. Energy* 274 (2020) 115261, <https://doi.org/10.1016/j.apenergy.2020.115261>
- [65] Z. Song, T. Liu, Y. Liu, X. Jiang, Q. Lin, Study on the optimization and sensitivity analysis of CCHP systems for industrial park facilities, *Int. J. Electr. Power Energy Syst.* 120 (2020) 105984, <https://doi.org/10.1016/j.ijepes.2020.105984>
- [66] Y. Chen, J. Chen, C. Liu, G. Liu, M. Ferrari, A. Sundararajan, Integrated modeling and optimal operation of multi-energy system for coastal community, in: 2023 IEEE International Conference on Electro Information Technology (eIT), 2023, pp. 211–216, <https://doi.org/10.1109/eIT57321.2023.10187307>
- [67] N.A. El-Taweel, H. Khani, H.E.Z. Farag, Hydrogen storage optimal scheduling for fuel supply and capacity-based demand response program under dynamic hydrogen pricing, *IEEE Trans. Smart Grid* 10 (4) (2018) 4531–4542, <https://doi.org/10.1109/TSG.2018.2863247>

- [68] Bloom Energy, Bloom electrolyzer data sheet, 2022, Available at <https://www.bloomenergy.com/wp-content/uploads/bloom-energy-electrolyzer-datasheet-december-2023.pdf>.
- [69] U.S. Department of Energy, DOE hydrogen and fuel cells program record, 2020, Available at <https://www.hydrogen.energy.gov/docs/hydrogenprogramlibraries/pdfs/20004-cost-electrolytic-hydrogen-production.pdf?Status=Master>.
- [70] A. Christensen, Assessment of hydrogen production costs from electrolysis: United States and Europe, Tech. Rep., International Council on Clean Transportation, 2020.
- [71] Y. Chen, M. Hu, Swarm intelligence-based distributed stochastic model predictive control for transactive operation of networked building clusters, *Energy Build.* 198 (2019) 207–215, <https://doi.org/10.1016/j.enbuild.2019.06.010>
- [72] Y. Chen, B. Park, X. Kou, M. Hu, J. Dong, F. Li, K. Amasyali, M. Olama, A comparison study on trading behavior and profit distribution in local energy transaction games, *Appl. Energy* 280 (2020) 115941, <https://doi.org/10.1016/j.apenergy.2020.115941>
- [73] W. Cole, A. Karmakar, Cost projections for utility-scale battery storage: 2023 update, Tech. Rep. NREL/TP-6A40-85332, National Renewable Energy Laboratory, 2023.
- [74] W. Cole, A.W. Frazier, C. Augustine, Cost projections for utility-scale battery storage: 2021 update, Tech. Rep., Golden, CO: National Renewable Energy Laboratory. NREL/TP-6A20-79236, 2021.
- [75] A. Smallbone, Levelised cost of storage for pumped heat energy storage in comparison with other energy storage technologies, *Energy Convers. Manag.* 152 (2017) 221–228, <https://doi.org/10.1016/j.enconman.2017.09.047>
- [76] F. Odoi-Yorke, A. Woagnon, Techno-economic assessment of solar PV/fuel cell hybrid power system for telecom base stations in Ghana, *Cogent Eng.* 8 (1) (2021) 1911285, <https://doi.org/10.1080/23311916.2021.1911285>
- [77] Storage tank costs: storing oil, energy, water and chemicals? Available at <https://thundersaidenergy.com/downloads/storage-tank-costs-storing-oil-energy-water-and-chemicals/>.
- [78] T. Weather Company, Wilmington, NC weather history, 2024, Available at <https://www.wunderground.com/history/daily/us/nc/wilmington/KILM/date/2023-1-1>.
- [79] National Solar Radiation Database (NSRDB), 2021, Available at <https://www.ncei.noaa.gov/data/nsrdb-solar/access/solar-only/>.
- [80] NREL, Marine energy atlas, 2024, Available at <https://maps.nrel.gov/marine-energy-atlas?vL=OmniDirectionalWavePowerMerged>.
- [81] Department of Energy, Commercial and residential hourly load profiles for all tmy3 locations in the United States, 2022, Available at <https://openei.org/datasets/files/961/pub/>.
- [82] N.A. El-Tawee, H. Khani, H.E.Z. Farag, Hydrogen storage optimal scheduling for fuel supply and capacity-based demand response program under dynamic hydrogen pricing, *IEEE Trans. Smart Grid* 10 (4) (2019) 4531–4542, <https://doi.org/10.1109/TSG.2018.2863247>
- [83] Idaho Department of Environmental Quality, Guidance for determining equalization water storage for public water systems, 2024, Available at <https://www2.deq.idaho.gov/admin/LEIA/api/document/download/4791>.
- [84] Snyder & Associates, Community water storage solutions: how to select a water tank, 2024, Available at <https://www.snyder-associates.com/community-water-storage-solutions-how-to-select-a-water-tank/>.
- [85] J. Park, S. Kang, S. Kim, H. Kim, S.-K. Kim, J.H. Lee, Optimizing green hydrogen systems: balancing economic viability and reliability in the face of supply-demand volatility, *Appl. Energy* 368 (2024) 123492, <https://doi.org/10.1016/j.apenergy.2024.123492>